Micromagnetic insight into a magnetoreceptor in birds: Existence of magnetic field amplifiers in the beak

Ilia A. Solov'yov* and Walter Greiner
Frankfurt Institute for Advanced Studies, Johann Wolfgang Goethe Universität, Ruth-Moufang-Strasse 1, 60438 Frankfurt-am-Main, Germany

(Received 15 June 2009; revised manuscript received 31 August 2009; published 14 October 2009)

The Earth's magnetic field provides an important source of directional information for many living organisms, especially birds, but the sensory receptor responsible for magnetic field detection still has to be identified. Recently, magnetic iron oxide particles were detected in dendritic endings of the ophthalmic nerves in the skin of the upper beak of homing pigeons and were shown to fulfill the special prerequisites of a biological receptor. Here we study the proposed receptor theoretically and formulate the criteria for which it becomes operational and can be used for registering the weak magnetic fields as, e.g., the geomagnetic field, by a bird.

DOI: 10.1103/PhysRevE.80.041919 PACS number(s): 87.19.−j, 75.10.Dg, 75.50.Gg, 75.60.Ch

I. INTRODUCTION

The ability of birds [1–7] and some other animals [2,8–11] to sense the geomagnetic field and use it for navigation remains a fascinating and intriguing problem in all branches of life sciences. Although there is no dispute that magnetic sense exists in avian, it is a controversial and not a well-understood phenomenon. Presently there is an ongoing debate whether magnetoreception in birds is based on a magneto-optically triggered chemical reaction [3,10,12–21] occurring in the eye, the interaction of magnetic microparticles in the beak [10,15,22–33], or both [6,34].

During the last decades there were many attempts to explain magnetoreception phenomenon qualitatively (see, e.g., Refs. [3,12–18,21,24,25,31,33,35–42]). However, at present, there is no theory which could describe all experimental observations at once. The magnetoreception mechanisms are usually studied qualitatively, whereas a systematic quantitative understanding is often necessary for the interpretation of existing experiments and for suggesting new ones. In this paper we make a step to fill this gap. Here we investigate the iron-mineral-based magnetoreception mechanism, which was motivated by recent experimental findings [22,23,27–29,32] and was theoretically described in Refs. [24–26]. In the present paper we go beyond the qualitative analysis performed in the papers cited above and present an in-depth investigation of the magnetoreception mechanism based on realistic quantitative calculations.

Magnetic iron oxide particles were detected in dendritic endings of the ophthalmic nerve in the skin of the upper beak of homing pigeons and were shown to fulfill the special prerequisites of a biological receptor [22,23,27–29,32]. The iron oxide particles in the beak were detected in different forms. Most prominent is the occurrence of tiny platelets of a well-defined shape and size. The platelets form straight chains as illustrated in Fig. 1 and are aligned preferentially along the dendrites. According to the x-ray absorption near-edge fine structure (XANES) data the platelets consist of a ferrimagnetic mineral maghemite and are most probably of single-crystalline nature [22,23,27–29]. The chain of maghemite platelets attracts a cluster of magnetite nanoparticles, which is connected to the nerve cell membrane [22–29]. A chain of maghemite platelets with a magnetite cluster build up a single magnetoreceptor unit [22,23,27–29]. There are many of these units in the beak, which react similar to the changes in external magnetic field.

Each maghemite platelet has a quadratic base of roughly 1×1 μm and a thickness of ~0.1 μm (see Fig. 1), but very little is known about their magnetic properties. The magnetization of a platelet is an important characteristic because it determines the interaction forces between magnetic constituents of a dendrite and plays a central role in the transducer mechanism of the geomagnetic field in birds [24–26,35].

The magnetization of a single platelet was studied computationally using the micromagnetic approach [29]. It was demonstrated that an isolated platelet has four magnetic domains, as shown in Fig. 1, and possesses zero magnetization.

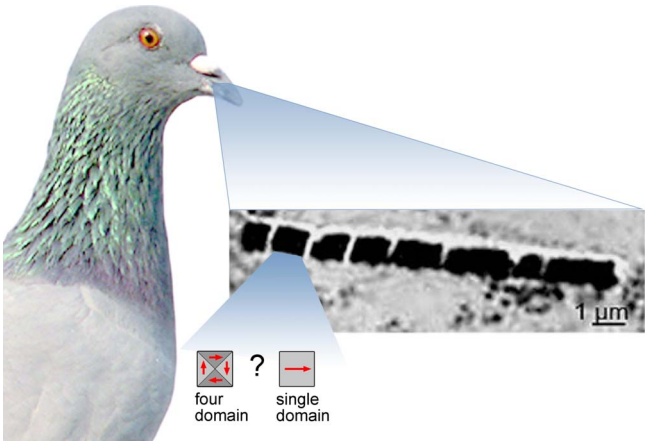

FIG. 1. (Color online) A chain of maghemite platelets detected by the transmission electron microscopy imaging method in the beak of homing pigeons [23] is of central importance for the magnetoreceptor organ in birds. The functioning of the magnetoreceptor depends on the total magnetization of the chain and thus on the magnetic domain structure of the individual platelets. Two possible domain distributions (four domain and a single domain) are discussed.

*Electronic address: ilia@fias.uni-frankfurt.de

A platelet may become magnetized in external magnetic field by shifting the walls of the magnetic domains. In Ref. [33] it was suggested that magnetic field of the Earth may be sufficiently strong to induce a noticeable transformation of the domain structure of the maghemite platelets in the bird's beak. The theoretical evaluation of this hypothesis is one of the central focuses of this paper.

We study how the total magnetization of the maghemite platelet chain depends on the number of platelets in the system. Based on the results of the calculation we formulate the criteria at which the magnetoreceptor suggested in [23,24] becomes operational. We demonstrate that the structures in the beak can work as an efficient magnetic field amplifier, which enhances the weak geomagnetic field leading to a significant magnetization of the chain, comparable with the saturation magnetization of the material. In the latter case the chain of maghemite platelets is expected to induce a noticeable effect on the nerve cell membrane in the bird's beak as suggested in Refs. [24–26,35].

Note that in earlier studies [24–26,35] we used a rough estimate for the magnetization of a maghemite platelet, which allows to describe the magnetoreceptor in birds in less details. We used the known value of the remanent magnetization of maghemite, which provides the low border estimate for the forces arising between magnetic particles in the dendrite. Nevertheless, the forces were shown to be sufficient to excite specific mechanoreceptive membrane ion channels. The present paper is aimed to quantify the model described in Refs. [24–26,35]. The results of the calculations demonstrate that at certain conditions the magnetization of the maghemite platelets is expected to be several times larger than was assumed earlier leading to a significant enhancement in magnetoreception by a bird.

II. THEORETICAL METHODS

A. Micromagnetic computation

In this section we describe the micromagnetic approach [43–45], which was used to calculate the distribution of magnetic domains in the magnetoreceptor. In the framework of this method the system is subdivided into smaller elements of volume $V_{\mathbf{r}}$ characterized by a vector $\mathbf{r}$. The volume $V_{\mathbf{r}}$ contains $N \gg 1$ elementary magnetic moments $\boldsymbol{\mu}_i$, $i=1,\ldots,N$, but is small enough to ensure that the elementary magnetic moments inside of it are almost collinear. Thus, we define the magnetization vector $\mathbf{M}(\mathbf{r})$ at point $\mathbf{r}$ as follows:

$$\mathbf{M}(\mathbf{r}) = \frac{1}{V_{\mathbf{r}}} \sum_{i=1}^{N} \boldsymbol{\mu}_i. \tag{1}$$

The magnetization vector $\mathbf{M}(\mathbf{r})$ in each element of the system can be written as

$$\mathbf{M}(\mathbf{r},t) = M_s \mathbf{m}(\mathbf{r},t), \tag{2}$$

where $\mathbf{m}(\mathbf{r},t) = m_x(\mathbf{r},t)\mathbf{e_x} + m_y(\mathbf{r},t)\mathbf{e_y} + m_z(\mathbf{r},t)\mathbf{e_z}$ is the magnetization unit vector (with $\mathbf{e_{x,y,z}}$ being the basis vectors of the coordinate frame) and M_s is the saturation magnetization of the sample.

At constant external magnetic field and temperature, the equilibrated state of the system corresponds to the minimum of its free energy. The free energy of the system sums from the exchange (F_{ex}), anisotropy (F_{an}), stray (F_{st}), and Zeeman (F_Z) interactions as follows:

$$F = F_{ex} + F_{an} + F_{st} + F_Z. \tag{3}$$

The exchange interaction is the basic interaction which causes cooperative magnetic ordering in a ferrimagnet (or ferromagnet). The contribution of the exchange interaction to the free energy of the system reads [43,44,46,47]

$$F_{ex} = \int_V A[(\nabla m_x)^2 + (\nabla m_y)^2 + (\nabla m_z)^2] dV. \tag{4}$$

Here the integration is performed over the volume of the system. A is the exchange constant, which can be particularized for different lattice geometries [44]. To understand the physical principles underlying Eq. (4) consider an example of the cubic lattice of spins, for which the interaction energy is given by the Heisenberg Hamiltonian [43,46,47]:

$$E_{ex} = -2J \sum_{i,j} \mathbf{S_i} \cdot \mathbf{S_j}. \tag{5}$$

Here the summation is performed over the neighboring spins. $\mathbf{S_i}$ and $\mathbf{S_j}$ are the spin angular momenta, expressed in units of $\hbar$, associated with spins i and j; J is the exchange integral. We assume that the interspin forces are sufficiently strong to keep the neighboring spins almost parallel. This approximation is valid for temperatures lower than the Curie temperature at which the magnetic ordering in a ferromagnet disappears.

Thus, if $\mathbf{S_i} = S\mathbf{m_i}$, and θ_{ij} is a small angle between the directions of $\mathbf{m_i}$ and $\mathbf{m_j}$, Eq. (5) can be rewritten as follows:

$$E_{ex} = -2JS^2 \sum_{i,j} \cos\,\theta_{ij} \approx -2JS^2 \sum_{i,j} \left(1 - \frac{\theta_{ij}^2}{2}\right)$$
$$= \text{const} + JS^2 \sum_{i,j} \theta_{ij}^2. \tag{6}$$

Since we are interested in the energy changes, we omit the constant term in Eq. (6). For small θ_{ij}, the condition $|\theta_{ij}| \approx |\mathbf{m_j} - \mathbf{m_i}|$ holds and Eq. (6) reads as

$$E_{ex} \approx JS^2 \sum_{i,j} (\mathbf{m_j} - \mathbf{m_i})^2. \tag{7}$$

The displacement vector $\mathbf{m_j} - \mathbf{m_i}$ can be expressed in terms of a continuous function $\mathbf{m}(\mathbf{r},t)$ defined in Eq. (2) as

$$\mathbf{m_j} - \mathbf{m_i} = (\Delta \mathbf{r_j} \cdot \nabla)\mathbf{m}, \tag{8}$$

where $\Delta \mathbf{r_j} = \mathbf{r_j} - \mathbf{r_i}$ is the position vector of spin j with respect to spin i. Substituting Eq. (8) into Eq. (7) one obtains

$$E_{ex} = JS^2 \sum_{i,j} [(\Delta \mathbf{r_j} \cdot \nabla)\mathbf{m}]^2 = JS^2 \sum_{i,j} [(\Delta \mathbf{r_j} \cdot \nabla m_x)^2$$
$$+ (\Delta \mathbf{r_j} \cdot \nabla m_y)^2 + (\Delta \mathbf{r_j} \cdot \nabla m_z)^2]. \tag{9}$$

By summing over j, multiplying the expression by the number of spins per unit volume, and clubbing all constants together, one obtains the exchange energy density per unit volume ε_{ex}:

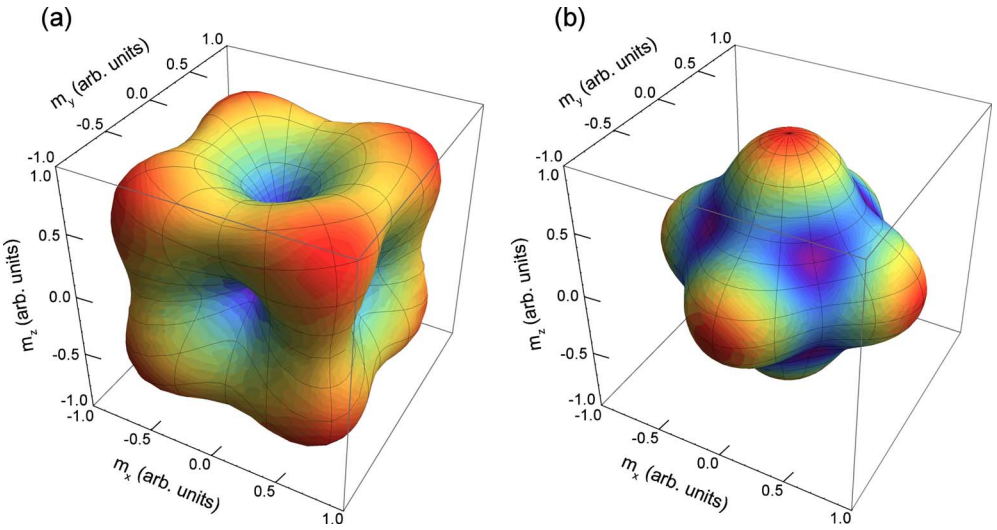

FIG. 2. (Color online) Cubic anisotropy energy density calculated from Eq. (13). Plot (a) shows the energy density distribution in which the coordinate axes are the easy axes ($K_0=0.3$, $K_1=3.0$). Plot (b) shows the energy distribution in which the coordinate axes are the hard axes ($K_0=1$, $K_1=-1.0$). The values of K_0 and K_1 are chosen in arbitrary units

$$\varepsilon_{ex} = A[(\nabla m_x)^2 + (\nabla m_y)^2 + (\nabla m_z)^2]. \tag{10}$$

Here $A=JS^2c/a$ is a constant [43], with a being the unit-cell edge length, and c is a number, equal to 1, 2, or 4, for the simple cubic, body-centered-cubic, or face-centered-cubic lattice, respectively. Typical values of A are on the order of 10^{-11} J/m. By integrating the exchange energy density over the volume of the system one obtains the contribution of exchange interactions to the free energy of the system.

In ferromagnetic and ferrimagnetic bodies one usually has to account for magnetic anisotropy effects, which arise because of the certain crystalline symmetry. In particular, in the absence of external magnetic field, some materials tend to be magnetized along a preferential direction, which in literature is usually referred to as the "easy direction" [43,46,47]. The anisotropic effects can be accounted for by means of an additional phenomenological term in the free-energy functional, F_{an}, as introduced in Eq. (3).

The magnetization unit vector $\mathbf{m}(\mathbf{r},t)$, Eq. (2), can be expressed in spherical coordinates by means of the angles θ and ϕ such that

$$\mathbf{m} = (\sin\vartheta\cos\varphi;\sin\vartheta\sin\varphi;\cos\theta). \tag{11}$$

Thus, the anisotropy energy density $\varepsilon_{an}(\mathbf{m})$ can be considered as a function of the spherical angles ϑ and φ and the contribution to the anisotropy free energy reads as

$$F_{an}(\mathbf{m}) = \int_V \varepsilon_{an}(\mathbf{m})dV. \tag{12}$$

From Eq. (12) follows, that the easy directions of the system correspond to the minima of the anisotropy energy density, whereas saddle points and maxima of $\varepsilon_{an}(\mathbf{m})$ determine the medium-hard axes and the hard axes, respectively. In many crystals, for example, maghemite or magnetite, the anisotropy energy density has cubic symmetry, which in Cartesian coordinates can be expanded as follows [43,46,47]:

$$\varepsilon_{an} = K_0 + K_1(m_x^2m_y^2 + m_y^2m_z^2 + m_z^2m_x^2) + K_2m_x^2m_y^2m_z^2 + \cdots, \tag{13}$$

where $K_0, K_1, K_2, \ldots$ are the expansion coefficients. The terms in Eq. (13) of the fourth order and greater are usually neglected because they have a minor impact on the structure and energy of the crystal (i.e., $K_2=0$, etc). From Eq. (13) follows, that if $K_1>0$, the anisotropy energy density ε_{an} has six equivalent minima corresponding to the directions x,y,z. Conversely, if $K_1<0$ there are eight equivalent minima along the directions pointing to the vertices of the cube and the coordinate axes directions become now hard axes. To illustrate this in Fig. 2 we plot the cubic anisotropy energy density calculated with $K_0=0.3$, $K_1=3.0$, plot (a), and $K_0=1$, $K_1=-1.0$, plot (b). The minima corresponding to the easy axes can be clearly seen. Note that the values of K_0 and K_1 in Fig. 2 are chosen in arbitrary units in order to illustrate the anisotropy energy density at different conditions.

The stray interaction term F_{st} in Eq. (3) is another important part of the magnetic interaction describing the classical long-range interactions between the magnetic moments of the body. The stray field is nonlocal because at a given location it depends on the magnetization of all other parts of the sample. The stray contribution to the free energy (in the cgs system of units) can be written as [43,44,46]

$$F_{st} = \int_V \varepsilon_{st}dV = -\frac{1}{8\pi}\int_V \mathbf{H_{st}}(\mathbf{r},t)\mathbf{M}(\mathbf{r},t)dV, \tag{14}$$

where $\mathbf{H_{st}}(\mathbf{r},t)$ is the demagnetizing field and $\mathbf{M}(\mathbf{r},t)$ is defined in Eq. (2). Accounting for the stray field is the most cumbersome part of the calculation. The complexity arises from the nonlocal nature of the stray energy term. The demagnetizing field $\mathbf{H_{st}}$ at location $\mathbf{r}$ is given by [43,44,46]

$$\mathbf{H}_{\mathrm{st}} = -\int_{V'} \frac{(\mathbf{r}-\mathbf{r}')\,\nabla\cdot\mathbf{M}(\mathbf{r}')}{|\mathbf{r}-\mathbf{r}'|^3} dV' + \oint_S' \frac{(\mathbf{r}-\mathbf{r}')\mathbf{n}\cdot\mathbf{M}}{|\mathbf{r}-\mathbf{r}'|^3} dS', \tag{15}$$

where $\mathbf{n}$ denotes the normal vector to the surface and S is the surface area of the sample.

The last contribution to the free energy of the system is the Zeeman energy term, which corresponds to the fourth summand in Eq. (3). The Zeeman interaction describes the influence of external magnetic field on the spins in the system. From basic electrodynamic calculations follows [47]

$$E_Z = \int_V \varepsilon_Z dV = -\frac{1}{4\pi}\int_V \mathbf{M_s}(\mathbf{r},t)\mathbf{B_0} dV, \tag{16}$$

where $\mathbf{B_0}$ is the external magnetic field.

B. Structure relaxation procedure

To describe the time evolution of the magnetization $\mathbf{M}(\mathbf{r},t)$ in the system and to determine the magnetization at equilibrium one has to solve the Landau-Lifshitz equation [43,45–48]

$$\frac{d\mathbf{M}}{dt} = -\gamma\mathbf{M}\times\mathbf{H}_{\mathrm{eff}} - \frac{\gamma\alpha}{M_s}\mathbf{M}\times(\mathbf{M}\times\mathbf{H}_{\mathrm{eff}}), \tag{17}$$

where $\mathbf{H}_{\mathrm{eff}}$ is the effective magnetic field at site $\mathbf{r}$, γ is the Landau-Lifshitz gyromagnetic ratio, and α is the Landau-Lifshitz phenomenological damping parameter, which is material dependent. The effective field is defined as

$$\mathbf{H}_{\mathrm{eff}} = -4\pi\frac{\partial F}{\partial \mathbf{M}}. \tag{18}$$

Here F is the free energy of the system calculated using Eq. (3).

To calculate the equilibrium distribution of magnetic domains in the chain of maghemite platelets the following procedure was used. The chain was subdivided into smaller elements with a predefined distribution of magnetic moments. The time evolution of the magnetization in each cell was described using the Landau-Lifshitz equation, Eq. (17). The second term in this equation describes the damping in the system, which leads to the formation of stable magnetic domains.

The relaxation time of the system depends on the damping parameter α. Since we are interested in the distribution of magnetic domains at equilibria, we assume $\alpha=0.5$, which leads to a faster relaxation in the system. In ferromagnetic and ferrimagnetic crystals the damping parameter is usually 0.01…0.1 [49,50] and is important for the study of dynamical processes in the system, while it has no impact on the equilibrated structure. To study the equilibrated structure of the system it is convenient to choose a larger value of α because the micromagnetic calculation converges faster to the stable configuration. Thus, to save the computation time, we use an increased value of the damping parameter as compared to the realistic values.

TABLE I. Parameters for maghemite used in the micromagnetic calculations. Different sets of parameters are available from the literature. (*) marks the value of the saturation magnetization used in the present paper.

Physical quantity	Symbol	Value	Reference
Saturation magnetization	M_s	300–417 (kA/m)	[29,54–57]
		$^{(*)}$375 (kA/m)	[29,56,57]
Exchange energy constant	A	13 (pJ/m)	[29]
Anisotropy constant	K_1	4.7 (kJ/m^3)	[52,53]
Anisotropy type		Cubic	[29,52,53]

III. RESULTS AND DISCUSSION

Using the methods described in the previous section we studied the energy and magnetization of the microplatelet chains of different lengths. The computations were performed with the use of the OOMMF program [51]. For a given number of platelets we consider several possible distributions of magnetic domains in the system and study the influence of the geomagnetic field on the stable configurations.

The material-dependent parameters used in the computations are known from the literature [29,52–54] and are compiled in Table I. According to the XANES data the platelets in the beak consist of a ferrimagnetic mineral maghemite [22,23,27–29]. The micromagnetic parameters for maghemite in Table I were taken from Refs. [29,52–57]. Recently an alternative hypothesis was discussed that the platelets may be composed of a different magnetic mineral (probably magnetite) [58]. However, this has a minor impact on the theory and results of the present paper because the parameters for maghemite are close to those for magnetite and some other magnetic iron oxides. The micromagnetic parameters for magnetite can be found in, e.g., Refs. [59–62].

In this paper we consider a chain of maghemite platelets in an external magnetic field directed along the chain. In Fig. 3 we illustrate the geometry of the magnetoreceptor and indicate the associated coordinate frame. Note, that strictly speaking a magnetoreceptor includes a chain of maghemite platelets and a magnetite cluster as was introduced in Ref. [24]. In this paper, for the sake of simplicity, we refer to a chain of maghemite platelets as to a magnetoreceptor.

Figure 4 shows the equilibrated structures calculated for chains with $N=1,\ldots,7$ platelets. For the calculation the system was subdivided into cubic elements of 10×10

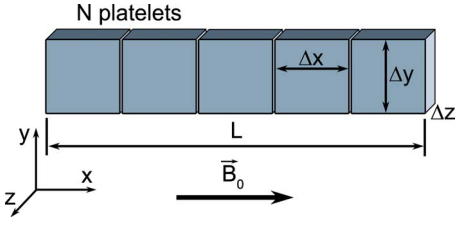

FIG. 3. (Color online) A schematic presentation of the maghemite platelet chain with N platelets. The length of the chain is L, while the length, the width, and the thickness of an individual platelet is Δx, Δy, and Δz, respectively. The external magnetic field $\vec{B}_0$ is applied along the chain, which is chosen as the x axis.

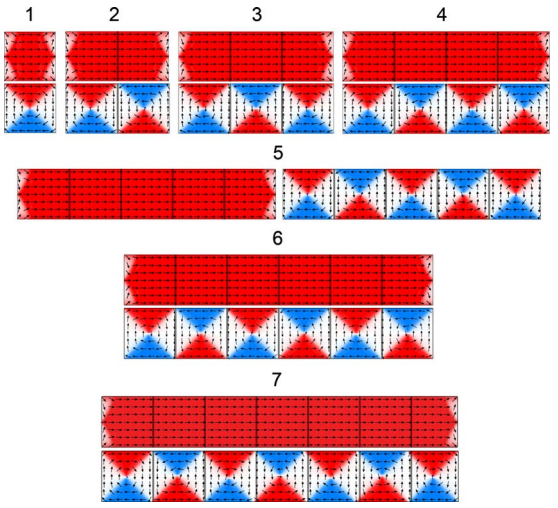

FIG. 4. (Color online) Distribution of magnetic domains in chains of maghemite platelets with different number of platelets. The figure shows stable configurations obtained with the use of the relaxation procedure described in Sec. II B. For each chain length the so-called 1D and 4D configurations are considered (see text). The number of platelets in the chain is given near the image of the corresponding structure. For the computation the system was subdivided into cubic elements of $10\times10\times10$ nm^3 and the external magnetic field of 0.5 G is directed along the chain.

$\times10$ nm^3. This subdivision has been chosen to fulfill the requirement of the micromagnetic calculation such that the elementary magnetic moments inside each element are almost collinear. With a $10\times10\times10$ nm^3 subdivision this condition is well preserved because the critical size of a single domain in magnetite is expected to be 60 ± 10 nm [36,63]. The characteristic size of a single domain in maghemite should be close to the value for magnetite, as the magnetic properties for both minerals are similar [56]. In order to check to which extent the $10\times10\times10$ nm^3 subdivision can be used in micromagnetic calculation, in Table II we present the total energies of a single maghemite platelet calculated using Eq. (3) by subdividing the platelet into cubic elements of different sizes. In this calculation the platelet has four triangular-shaped domains as shown in Fig. 4. The smallest subdivision considered corresponds to the $4\times4\times4$ nm^3 cell containing ~500 iron atoms as follows from the bulk density of maghemite [56]. This cell size is more than an order of magnitude smaller than the critical size of a single domain, and therefore the corresponding subdivision is expected to give reliable results. It is difficult to perform micromagnetic computations by subdividing the system into smaller elements, as the total number of cells in the case of a $4\times4\times4$ nm^3 subdivision of a single maghemite platelet is already more than 1.5×10^6, as follows from Table II, requiring significant computation time and power. Increasing the cell size results in the increase in the total energy of the platelet and in the decreasing accuracy of the calculation (see Table II). From Table II follows that the relative deviation of energy from the value calculated for a platelet subdivided into $4\times4\times4$ nm^3 cells is less than a percent for the platelet subdivided into cells of $10\times10\times10$ nm^3 (or of smaller size) and about 3% for the $20\times20\times20$ nm^3 subdivision. This fact shows that $10\times10\times10$ nm^3 and $20\times20\times20$ nm^3 subdivisions are accurate enough and can be used for the computations.

TABLE II. The total energy of a single maghemite platelet calculated using Eq. (3) subdivided into cubic elements (cells) of different sizes. The relative error shows the deviation of energy from the value calculated for a platelet subdivided into cells of $4\times4\times4$ nm^3. The last column in the table gives the total number of cells in the corresponding computation. In this calculation the platelet has four triangular-shaped domains as shown in Fig. 4.

Cell size (nm×nm×nm)	Energy (eV)	Relative error (%)	Number of cells
$4\times4\times4$	856.24		1562500
$5\times5\times5$	857.05	0.09	800000
$10\times10\times10$	861.45	0.60	100000
$20\times20\times20$	880.32	2.8	12500

The external magnetic field is assumed to be equal to the typical geomagnetic field of 0.5 G directed along the chain (see Fig. 3). In the present paper we focus on this particular example in order to demonstrate that the geomagnetic field is sufficient to induce a noticeable change in the magnetization of the platelet chain leading to magnetoreception of a bird. We describe the key aspects of the iron-mineral-based magnetoreception mechanism and support our rationale with calculations. We perform a detailed analysis of the magnetoreceptor at a fixed intensity and orientation of the external magnetic field, while the study at different conditions is left open for further consideration.

For each chain size two magnetic isomers were considered, which we refer to as the one domain (1D) and the four domain (4D) configurations. The isomers are classified according to the distribution of magnetic domains in the structures prior to the relaxation procedure: in the 1D isomers each platelet has a single domain with the magnetization directed along the chain. In the 4D isomers each platelet is assumed to have four circular domains as illustrated in Fig. 1. We considered two possible magnetic isomers of the chains because other configurations are expected to have significantly higher energies than the structures shown in Fig. 4 and therefore are unlikely to be observed.

Figure 4 shows that the relaxed 1D configurations acquire four domains in the outermost platelets, while inside the chain the magnetic moments form single domains. The domains in the 4D configurations do not change significantly in the course of the relaxation process.

To simplify the computation we neglected the small distances between the individual platelets and considered the chains of maghemite platelets as solid magnetic bars. This assumption has minor influence on the results of the computation because the distances between the platelets are significantly smaller than the characteristic size of the platelets and in some cases can even not be resolved in electron microscope (see Fig. 1).

An important characteristic of the maghemite platelet chain is the total magnetization of the system. In Fig. 5 we show the relative magnetization calculated for structures

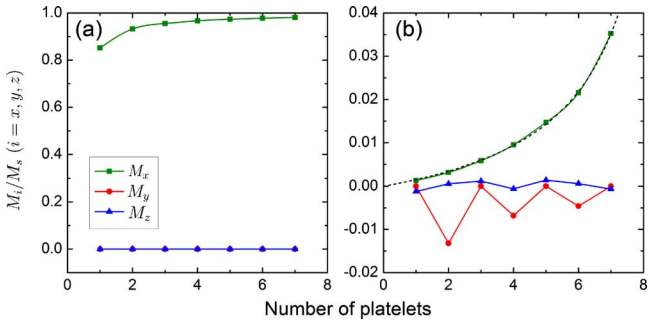

FIG. 5. (Color online) Relative magnetization of the maghemite platelet chains shown in Fig. 4. Plot (a): components of the magnetization vector calculated for the 1D structures; plot (b): components of the magnetization vector calculated for the 4D structures. The values are normalized to the saturation magnetization of maghemite given in Table I. The dashed curve in (b) was calculated using Eq. (21) and illustrates the magnetic field amplification mechanism in the system.

shown in Fig. 4 as a function of the number of platelets in the chain. Figures 5(a) and 5(b) show the components of the magnetization vector calculated for the 1D and 4D structures, respectively. The values are normalized to the saturation magnetization of maghemite given in Table I.

As seen from Fig. 5(a) the components of the magnetization for the 1D structure along the chain, M_x, steadily approach the saturation limit. Small deviations are due to the domains at the edge of the chain (see Fig. 4). As follows from Fig. 4, the magnetization in the 1D structures is symmetrical with respect to the chain axis. Therefore, the perpendicular components of the magnetization vector, M_y and M_z, are close to zero.

The magnetization of the 4D structures is significantly smaller than the magnetization of the 1D structures [see Fig. 5(b)]. Figure 5(b) shows that in the geomagnetic field the magnetization of the chains with less than seven platelets is below 5% of the saturation value. However, the magnetization along the chain, M_x, for the 4D configuration steadily grows with increasing number of platelets in the system. This happens because the external magnetic field is amplified by the platelets enhancing the total magnetization of the chain.

The magnetization of the chain in the direction of the external magnetic field is proportional to the length of the chain L and to the strength of the external magnetic field B_0 (see Fig. 3). Thus, the component of the magnetization in that direction, M_x, reads as

$$M_x = a_0(B_0 + B_{eff})L = a_0(B_0 + B_{eff})\Delta x N, \tag{19}$$

where a_0 is the proportionality constant, Δx is the length of a platelet (see Fig. 3), N is the total number of platelets, and B_{eff} is the effective magnetic field created by the magnetized chain. The magnetization of a chain cannot exceed the saturation value. If $M_x \ll M_s$ the linear approximation can be used in which the effective magnetic field is proportional to the magnetization of the chain:

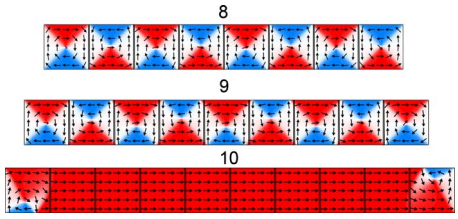

FIG. 6. (Color online) Calculated distributions of magnetic domains in chains with eight, nine, and ten maghemite platelets. Prior to relaxation all platelets were assumed to have four equally sized circular magnetic domains. The external magnetic field of 0.5 G is applied along the chain. For the computation the system was subdivided into cubic elements of $20 \times 20 \times 20$ nm^3.

$$B_{eff} = \frac{1}{\beta} M_x. \tag{20}$$

Here β is the proportionality constant. In the case of $M_x \leq M_s$, the approximation Eq. (20) becomes invalid because one has to account for nonlinear effects in the $B_{eff}(M_x)$ dependence. Substituting Eq. (20) into Eq. (19) and rearranging the terms one obtains

$$M_x = \frac{a_0 \Delta x B_0 N}{1 - \frac{a_0 \Delta x}{\beta} N} = \frac{\beta B_0 N}{(\beta / a_0 \Delta x) - N} = \beta \frac{B_0 N}{N_0 - N}. \tag{21}$$

As follows from Eq. (21) the magnetization of the chain increases as the number of platelets in the system grows. According to Eq. (21), at $N \to N_0$ the magnetization becomes infinitely large illustrating the fact that at certain length the 4D configuration of the chain is unstable and transforms to the 1D configuration.

Physically, this transition can be understood as follows: the external magnetic field magnetizes the chain, which in turn results in the creation of an effective magnetic field inside the chain, which is collinear with the external magnetic field. The resulting magnetic field shifts the magnetic domain walls increasing the size of the domains with the magnetization directed parallel to the external magnetic field. At certain length the effective magnetic field reaches a threshold value, at which the 4D structure becomes strongly distorted and therefore unstable (see Fig. 6).

The critical number of platelets at which the 4D $\to$ 1D structural transition occurs can be estimated from Eq. (21). Assuming the threshold value of magnetization at which the 4D configuration becomes unstable to be equal M_{thr} one obtains

$$N_{crit} \geq N_0 \frac{1}{1 + (\beta B_0 / M_{thr})}. \tag{22}$$

N_{crit} in Eq. (22) is an integer and it may be smaller than N_0 if the external magnetic field is sufficiently large. The threshold value of the magnetization $M_{thr} \leq M_s$, where M_s is the saturation magnetization of maghemite, is defined in Table I.

The dashed curve in Fig. 5(b) is calculated using Eq. (21) and illustrates the magnetic field amplification mechanism in the system. We determined β and N_0 in Eq. (21) by fitting the

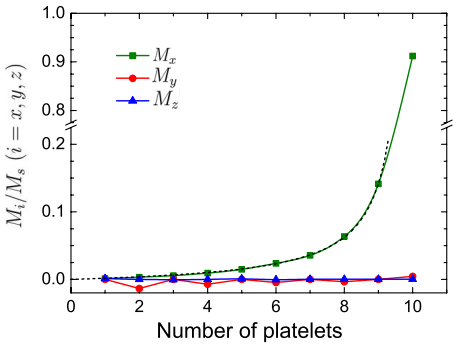

FIG. 7. (Color online) Relative magnetization calculated for the chains of maghemite platelets with $N \leq 10$. The structures with eight, nine, and ten platelets are shown in Fig. 6. In the micromagnetic calculation the system is subdivided into cubic elements of $20 \times 20 \times 20$ nm^3. The external magnetic field is directed along the chain being equal to 0.5 G.

calculated values for M_x with Eq. (21). The least-squares fitting method results in $\beta = 10^8$ A/m·T and $N_0 = 9.63$. Thus, the 4D→1D structural transition in a geomagnetic field of 0.5 G is expected in chains with more than ten platelets.

Micromagnetic calculations with a $10 \times 10 \times 10$ nm^3 subdivision of the system become computer time demanding for a chain with ten platelets because it involves 10^6 elements. Therefore, in order to study the domain structure of a chain with ten platelets we subdivided the system into $20 \times 20 \times 20$ nm^3 elements. Figure 6 shows the calculated stable distribution of magnetic domains in chains with 8, 9, and 10 platelets. The structure of the chains with 1…7 platelets in this case is similar to the structures computed with the $10 \times 10 \times 10$ nm^3 subdivision shown in Fig. 4. The structures shown in Fig. 6 were obtained with the use of the relaxation procedure described in Sec. II B. Initially, all platelets were assumed to have four equally sized magnetic domains and the external magnetic field of 0.5 G was applied along the chain (see Fig. 3).

Figure 6 shows that the distortion of magnetic domains in the system increases with increasing number of platelets in the chain: in the chain with eight platelets the size of domains in different platelets is close, while in the chain with nine platelets the domains are notably different in size. The chain with ten platelets undergoes the 4D→1D structural transition as predicted from Eq. (22). The 4D configuration in the chain with ten platelets is not stable and in the course of the relaxation process it transforms to the 1D state. If the external magnetic field is larger than 0.5 G, the 4D→1D structural transition occurs in shorter chains as predicted by Eq. (22).

The magnetization of the structures with $N = 1, \ldots, 10$ platelets is analyzed in Fig. 7. The three components of the magnetization vector are shown by squares, dots, and triangles. The dashed curve in Fig. 7 shows the magnetization along the chain calculated using Eq. (21) with $\beta = 1.16 \times 10^8$ A/m·T and $N_0 = 9.98$. The values of β and N_0 were calculated from the magnetization of the chains with 1…9 platelets using the least-squares fitting method.

In an external magnetic field of 0.5 G the 4D configuration in a chain with ten platelets is not stable. Therefore, the magnetization for this structure cannot be predicted using Eq. (21), as also illustrated in Fig. 7.

It is worth noting that the y component of the magnetization vector, M_y (the coordinate frame is shown in Fig. 3), in the 4D configurations is close to zero for chains with odd number of platelets and is slightly negative for chains with even number of platelets as can be seen from Figs. 5(b) and 7. This happens because the size of the domains with y-directed magnetization in the outermost platelets is slightly different from the size of the homothetic domains in the inner platelets of the chain. In the chains with an odd number of platelets the magnetization of the y-directed domains in the two outermost platelets cancel each other because the domains are equally sized and are oppositely directed (see Fig. 4). In this case there is an even number of y-directed domains inside the chain, which cancel each other pairwise.

In the chains with an even number of platelets, the magnetization of the y-directed domains in the two outermost platelets points in the positive y direction (see Fig. 4). The magnetization of the y-directed domains inside the chain is larger than the magnetization of the y-directed domains in the outermost platelets due to the stray field at the edge of the chain. Thus, in a chain with N platelets, $N-2$ domains inside the chain and two domains in the outermost platelets point in the positive y direction, while N domains point in the opposite direction. Consequently, in the chains with even number of platelets the y-directed domains do not cancel each other completely leading to a small negative value of the total magnetization of the chain in the y direction [see Figs. 5(b) and 7].

An important characteristic of the maghemite platelet chain is the total energy of the system defined in Eq. (3). Figure 8 shows the total energies calculated for structures with different distributions of magnetic domains as a function of the number of platelets in the chain. The calculated energies correspond to the stable configurations shown in Figs. 4 and 6. Squares show the energies calculated for the 1D configurations shown in Fig. 4. In this computation the chain was subdivided into $10 \times 10 \times 10$ nm^3 elements. Dots and triangles represent the results obtained for the 4D structures (see Figs. 4 and 6), which were subdivided into $10 \times 10 \times 10$ nm^3 and $20 \times 20 \times 20$ nm^3 elements, respectively.

Figure 8 shows that the 4D configurations are energetically favorable for short chains, while for chains with $N \geq 5$ the energy of the 1D configuration is lower. The energy difference between the 4D and the 1D configurations with $N > 5$ increases with the number of platelets, and, as follows from Eq. (22), at $N = 10$ the 4D configuration becomes unstable: in the course of the relaxation process the 4D configuration transforms to the 1D state. This is seen from Fig. 8, where the energy of a chain with ten platelets is considerably lower than the energy of the 4D configuration with nine platelets. Physically the transition at $N = 10$ can be viewed as follows: at $N = 10$ the energy difference between the 4D and the 1D configurations reaches a threshold value at which the external magnetic field of 0.5 G, amplified by the chain, causes the system in the 4D state to overcome the energy barrier separating the 4D and the 1D configurations and to populate the energetically favorable 1D state.

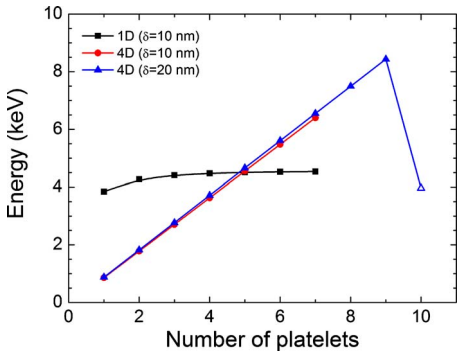

FIG. 8. (Color online) The total energy of the maghemite platelet chains calculated using Eq. (3) for structures with different distributions of magnetic domains as a function of the number of platelets in the system. The calculated energies correspond to the stable structures shown in Figs. 4 and 6. Squares show the energies calculated for the 1D configurations, while dots and triangles show the results obtained for the 4D configurations. For the micromagnetic computation the chains were subdivided into cubic elements of $10\times10\times10$ nm^3 (squares and dots) and $20\times20\times20$ nm^3 (triangles). The open triangle for $N=10$ corresponds to the energy calculated for the structure shown in Fig. 6. The energy for this structure is shown by a different symbol because the structure with $N=10$ cannot be considered as a 4D configuration, since in an external magnetic field of 0.5 G the 4D configuration in a chain with ten platelets is not stable.

For an efficient functioning of the magnetoreceptor, the chain of maghemite platelets in the beak should have a nonzero magnetization, which determines the force exerted on the nerve cell membrane as was demonstrated in Ref. [24]. Figure 5(a) shows that the 1D configurations always have magnetization close to the saturation value. The 1D configurations in chains with $N<5$ are energetically unfavorable compared to the 4D configurations (see Fig. 8). Therefore, the 4D configurations with $N<5$ are more likely to be observed in the beak. However, the magnetization of these configurations is less than 2% of the saturation value [see Fig. 5(b)], being not sufficient to produce a noticeable effect on the nerve cell membrane in the beak of a bird. Therefore, receptors with less than five platelets are expected to have a minor role in the magnetoreception process at normal conditions.

The energy of the chains with $5\leq N\leq9$ is lower for the 1D structures, which shows that the 1D configurations for these chain lengths are possible. However, depending on the growth conditions of the maghemite platelet chains the 4D structures with $5\leq N\leq9$ platelets may also occur, even being energetically unfavorable. Figure 5(b) shows that the 4D configurations with $5\leq N\leq9$ possess magnetization of about 1%–15% from the saturation value. Therefore, the magnetoreceptors with $5\leq N\leq9$ platelets in the 1D state will produce a strong response to the external magnetic field, while the receptors in the 4D state a relatively weak one.

For the chains with $N\geq10$ the 4D configurations become unstable and the chain of maghemite platelets acquires a significant magnetization close to the saturation magnetization of maghemite. Magnetoreceptors with $N\geq10$ are expected to induce a detectable impact on the nerve cell membrane. Since the magnetization of such structures is close to the saturation value, the forces transmitted to the nerve cell membrane are about an order of magnitude larger than those predicted in Ref. [24]. In that paper we used the value of the saturation magnetization of maghemite for estimating the transduced forces, which appears to be about eight times smaller than the value of the saturation magnetization.

It is also worth noting that chains with ten platelets were observed in the beak of birds. Figure 1 shows an electron microscope picture of a structure recorded in the beak of a homing pigeon [23], where ten platelets can be clearly identified. This fact supports strongly the idea that in the course of the natural evolution the magnetoreceptors in the beak have evolved to the sizes at which the magnetoreception is the most efficient.

IV. CONCLUSION

There is less and less doubt that the iron-mineral-based magnetoreception mechanism is related to the magnetic sense in birds [22,23,27–29,32]. During the last years this mechanism attracted significant attention because of the novel experimental measurements, which allowed to formulate the underlying theoretical concepts [24–26,35]. A recently developed model [24] was aimed to describe the magnetic field effects among iron-mineral containing particles in the beak.

In Refs. [22,23,27–29] it was experimentally demonstrated that the magnetoreceptor in the beak includes two components: magnetic clusters attached to the nerve cell membrane and chains of maghemite platelets aligned along the dendrites. The chains of maghemite platelets are of central importance for the magnetoreceptor organ in birds. The functioning of the magnetoreceptor depends on the magnetization of the chain and thus on the magnetic domain structure of the individual platelets. In earlier studies [24–26,35] we used an estimate for the magnetization of a maghemite platelet in order to describe the magnetoreceptor in birds. As it now turns out, this description has to be considered as qualitative. We had used the known value of the remanent magnetization of maghemite, which provides the low border estimate for the forces arising between magnetic particles in the dendrite. Nevertheless, the forces were shown to be sufficient to excite specific mechanoreceptive ion channels in the membrane.

In the qualitative description it is possible to understand the basic principles of the magnetoreception mechanism, but for an in-depth analysis a quantitative study is important. In this paper we went beyond the qualitative analysis and performed a detailed investigation of the magnetic properties of the maghemite platelets in a weak (i.e., the Earth's) external magnetic field. The results of the calculations demonstrate that at certain conditions the magnetization of the maghemite platelets is expected to be several times larger than was assumed earlier [24–26,35] leading to a significant enhancement in magnetoreception. Indeed, in Ref. [24] it was shown that the pull on the nerve cell membrane depends on the magnetization of the platelets. Therefore, increasing the magnetization results in the increase in the probability to

open specific mechanosensitive ion channels in the membrane.

In this paper we studied how the magnetization of the maghemite platelet chain depends on the number of platelets in the system. We demonstrated that the structures in the beak work as an efficient magnetic field amplifier, which enhances the weak geomagnetic field in the dendrite leading to a significant magnetization of the chain, comparable with the saturation magnetization of the material. We showed that chains with $N<5$ platelets have a minor impact on the magnetoreception because the magnetization of the chain in this case is negligibly small. For the chains with $N\geq 10$ we predict a strong response of the iron-mineral-based magnetoreceptor to the geomagnetic field. The forces acting on the nerve cell membrane in this case are about an order of magnitude larger than those discussed in Ref. [24]. Thus, the magnetoreceptor with ten (or more) platelets is expected to respond efficiently to the small variations in the magnetic field, which, for example, occur while moving through magnetic field anomalies.

This paper raises important questions for further theoretical and experimental investigations. We demonstrated that the number of platelets in the chain determines many properties of the magnetoreceptor. However, it is very unlikely that all magnetoreceptors in the beak are identical. More natural is that the number of platelets in different magnetoreceptors has a form of a distribution function, e.g., a Poisson or a Gauss distribution. Depending on the quantity of magnetoreceptors with one, two, etc. platelets the birds may respond to the external magnetic field, and its variations, in a different way. Another question, which can be addressed experimentally, is the elemental analysis of the individual platelets. Currently there is an ongoing debate about the constituent material of the platelets. According to the x-ray absorption near-edge fine structure data the platelets consist of maghemite [22,23,27–29], but there are also some alternative suggestions [58]. Using the energy dispersive x-ray spectroscopy method (see, e.g., Ref. [64]) it should be possible to determine the ratio of different elements in the platelet which would allow us to conclude about its material.

The paper opens a broad spectrum of questions for further theoretical consideration. Among others it is important to study how the increased external magnetic field (e.g., $B_0=1$, 3, 10 G,…) impacts on the magnetization of the maghemite platelet chains and therefore on the magnetoreception of a bird. Such analysis allows to determine the "magnetic window," i.e., the magnetic field intensities at which the magnetoreception mechanism is functioning properly.

In this paper we demonstrated that applying an external magnetic field along the maghemite platelet chain can induce a structural transition in the domain structure of the system. We considered an example of fixed field to illustrate the basic principles of the magnetic field amplification mechanism. In further investigation it is important to study how the reorientation of external magnetic field influences the magnetic domain structure of the platelet chain because this knowledge could link the iron-mineral-based magnetoreceptor with the compass sense in birds. Oblique magnetic field should also be investigated, as the geomagnetic field can make any angle with the chain axis.

Another step would be to study two- and three-dimensional arrays of chains instead of a single chain, as done in the present paper. This study is important, as in the dendrite, in the beak of a bird apparently there are several chains of platelets oriented roughly parallel to each other [22,23,27–29]. Interactions between the platelets from different chains such as the dipole-dipole interactions could affect the critical number of platelets in a chain at which the 4D configurations become unstable.

The results of the present paper also allow to study the influence of small variations in the external field on the magnetoreception mechanism. This is important for the understanding of avian behavior at magnetic field anomalies, where the birds usually become disoriented, but after a certain acclimation period can find the correct flight direction [65–67]. The study of oscillating electromagnetic fields is another important task, as it may lead to the suggestion of new experiments for probing of the iron-mineral-based magnetoreception mechanism in birds.

ACKNOWLEDGMENTS

This work was supported by the Stiftung Polytechnische Gesellschaft Frankfurt am Main and partially supported by the European Commission within the Network of Excellence project EXCELL. The use of the Frankfurt Center for Scientific Computing is also acknowledged. The authors thank Alexander Yakubovich for useful discussions.

[1] W. Wiltschko and R. Wiltschko, J. Exp. Biol. **199**, 29 (1996).
[2] R. Wiltschko and W. Wiltschko, Bioessays **28**, 157 (2006).
[3] C. T. Rodgers and P. J. Hore, Proc. Natl. Acad. Sci. U.S.A. **106**, 353 (2009).
[4] F. Merkel and W. Wiltschko, Vogelwarte **23**, 71 (1965).
[5] W. Wiltschko and F. Merkel, Verh. Dtsch. Zool. Ges. **59**, 362 (1966).
[6] H. Mouritsen and T. Ritz, Curr. Opin. Neurobiol. **15**, 406 (2005).
[7] D. Heyers, M. Manns, H. Luksch, O. Güntürkün, and H. Mouritsen, PLoS ONE **2**, e937 (2007).
[8] J. Lohmann and S. Johnson, Trends Neurosci. **23**, 153 (2000).
[9] M. Freake, R. Muheim, and J. Philips, Q. Rev. Biol. **81**, 327 (2006).
[10] S. Johnsen and K. J. Lohmann, Phys. Today **61** (3), 29 (2008).
[11] S. Begall, J. Červený, J. Neef, O. Vojtěch, and H. Burda, Proc. Natl. Acad. Sci. U.S.A. **105**, 13451 (2008).
[12] I. A. Solov'yov, D. Chandler, and K. Schulten, Biophys. J. **92**, 2711 (2007).
[13] T. Ritz, S. Adem, and K. Schulten, Biophys. J. **78**, 707 (2000).
[14] I. A. Solov'yov, D. E. Chandler, and K. Schulten, Plant Signal. Behav. **3**, 676 (2008).

[15] I. A. Solov'yov, Ph.D. dissertation, Johann-Wolfgang Goethe Universität, Frankfurt am Main, Deutschland, 2008.
[16] K. Maeda, K. B. Henbest, F. Cintolesi, I. Kuprov, C. T. Rodgers, P. A. Liddell, D. Gust, C. R. Timmel, and P. J. Hore, Nature (London) **453**, 387 (2008).
[17] T. Ritz, R. Wiltschko, P. Hore, C. T. Rodgers, K. Stapput, P. Thalau, C. R. Timmel, and W. Wiltschko, Biophys. J. **96**, 3451 (2009).
[18] I. A. Solov'yov and K. Schulten, Biophys. J. **96**, 4804 (2009).
[19] M. Liedvogel, K. Maeda, K. Henbest, E. Schleicher, T. Simon, C. R. Timmel, P. Hore, and H. Mouritsen, PLoS ONE **2**, e1106 (2007).
[20] F. Cintolesi, T. Ritz, C. Kay, C. Timmel, and P. Hore, Chem. Phys. **294**, 385 (2003).
[21] O. Efimova and P. Hore, Biophys. J. **94**, 1565 (2008).
[22] G. Fleissner, E. Holtkamp-Rötzler, M. Hanzlik, M. Winklhofer, G. Fleissner, N. Petersen, and W. Wiltschko, J. Comp. Neurol. **458**, 350 (2003).
[23] G. Fleissner, B. Stahl, P. Thalau, G. Falkenberg, and G. Fleissner, Naturwissenschaften **94**, 631 (2007).
[24] I. A. Solov'yov and W. Greiner, Biophys. J. **93**, 1493 (2007).
[25] I. A. Solov'yov and W. Greiner, Eur. Phys. J. D **51**, 161 (2009).
[26] I. A. Solov'yov and W. Greiner, in *Latest Advances in Atomic Cluster Collisions: Structure and Dynamics from the Nuclear to the Biological Scale*, edited by A. V. Solov'yov and J.-P. Connerade (Imperial College Press, London, 2008), pp. 377–388.
[27] B. Stahl, G. Fleissner, G. Falkenberg, and G. Fleissner, HASYLAB Annual Report, DESY, Hamburg, 2006, pp. 1289–1290 (unpublished).
[28] B. Stahl, G. Fleissner, G. Falkenberg, and G. Fleissner, in *Proceedings of the Fourth Fall Conference on Metalloproteins and Metalloidproteins*, edited by A. Kyriakopoulos, B. Michalke, A. Grabert, and D. Behne (Herbert Utz Verlag, München, 2006), pp. 63–68.
[29] B. Stahl, G. Fleissner, G. Falkenberg, and G. Fleissner, in *Proceedings of the XAFS13* (American Institute of Physics, New York, 2007), Vol. 882, pp. 755–757.
[30] A. F. Davila, M. Winklhofer, V. P. Shcherbakov, and N. Petersen, Biophys. J. **89**, 56 (2005).
[31] J. L. Kirschvink, M. M. Walker, and C. E. Diebel, Curr. Opin. Neurobiol. **11**, 462 (2001).
[32] M. Hanzlik, C. Heunemann, E. Holtkamp-Rötzler, M. Winklhofer, N. Petersen, and G. Fleisner, Biometals **13**, 325 (2000).
[33] G. Fleissner, G. Fleissner, B. Stahl, and G. Falkenberg, J. Ornithol. **148** (Suppl. 2), 643 (2007).
[34] W. Wiltschko and R. Wiltschko, J. Ornithol. **148** (Suppl. 1), 61 (2007).
[35] I. Solov'yov and W. Greiner, e-print arXiv:0704.1763 [physics.bio-ph].
[36] J. Kirschvink, D. Jones, and B. McFaden, *Magnetite, Biomineralization and Magnetoreception in Organisms* (Plenum, New York, 1985).
[37] T. Ritz, P. Thalau, J. B. Phillips, R. Wiltschko, and W. Wiltschko, Nature (London) **429**, 177 (2004).
[38] K. Wang and T. Ritz, Mol. Phys. **104**, 1649 (2006).
[39] M. Winklhofer, *Modelle Hypotethischer Magnetfeldrezeptoren Auf der Grundlage Biogenen Magnetits* (Verlag Merie Leidorf GmbH, Rahden, Westfallen, 1999), ISBN 3–89646–015–3.
[40] M. Winklhofer, Phys. Unserer Zeit **35**, 120 (2004).
[41] V. Shcherbakov and M. Winklhofer, Eur. Biophys. J. **28**, 380 (1999).
[42] M. Winklhofer, E. Holtkamp-Rötzler, M. Hanzlik, G. Fleissner, and N. Petersen, Eur. J. Mineral. **13**, 659 (2001).
[43] J. B. William Fuller, *Magnetostatic Principles in Ferromagnetism* (North-Holland, Amsterdam, 1962).
[44] R. Hertel and H. Kronmüller, Phys. Rev. B **60**, 7366 (1999).
[45] J. Fidler and T. Schrefl, J. Phys. D **33**, R135 (2000).
[46] G. Krinchik, *Physics of Magnetic Phenomena* (Moscow University Press, Moscow, 1976).
[47] L. Landau, L. Pitaevskii, and E. Lifshitz, *Electrodynamics of Continuous Media* (Elsevier/Butterworth-Heinemann, New York/London, 1984).
[48] W. F. J. Brown, *Micromagnetics* (Wiley, New York, 1963).
[49] C. D. Stanciu, A. V. Kimel, F. Hansteen, A. Tsukamoto, A. Itoh, A. Kiriliyuk, and Th. Rasing, Phys. Rev. B **73**, 220402(R) (2006).
[50] J. Fidler, T. Schrefl, W. Scholz, D. Suess, R. Dittrich, and M. Kirschner, J. Magn. Magn. Mater. **272-276**, 641 (2004).
[51] M. J. Donahue and D. G. Porter, *OOMMF User's Guide, Version 1.0, NISTIR 6376* (National Institute of Standards and Technology, Gaithersburg, MD, 1999).
[52] A. Cabot, A. P. Alivisatos, V. F. Puntes, L. Balcells, O. Iglesias, and A. Labarta, Phys. Rev. B **79**, 094419 (2009).
[53] H. Kachkachi, A. Ezzir, M. Nogues, and E. Tronc, Eur. Phys. J. B **14**, 681 (2000).
[54] C. Johansson, M. Hanson, M. Pedersen, and S. Morup, J. Magn. Magn. Mater. **173**, 5 (1997).
[55] R. Hergt, R. Hiergeist, I. Hilger, W. Kaiser, Y. Lapatnikov, S. Margel, and U. Richter, J. Magn. Magn. Mater. **270**, 345 (2004).
[56] C. Hunt, B. Moskowitz, and S. Banerjee, *Rock Physics and Phase Relations, A Handbook of Physical Constants (AGU Reference Shelf 3)* (American Geophysical Union, Washington, DC, 1995), pp. 189–204.
[57] D. Horák, F. Lednický, E. Petrovský, and A. Kapička, Macromol. Mater. Eng. **289**, 341 (2004).
[58] M. Winklhofer and J. L. Kirschvink, e-print arXiv:0805.2249.
[59] S. Xu and D. J. Dunlop, Geophys. Res. Lett. **23**, 2819 (1996).
[60] L. Afremov and A. Panov, Phys. Metals Metall. **86**, 269 (1998).
[61] S. Xu and D. J. Dunlop, J. Geophys. Res. **99**, 9035 (1994).
[62] K. Fabian, A. Kirchner, W. Williams, F. Heider, T. Leibl, and A. Huber, Geophys. J. Int. **124**, 89 (1996).
[63] R. F. Butler and S. K. Banerjee, J. Geophys. Res. **80**, 4049 (1975).
[64] V. Solovyeva, K. Keller, and M. Huth, Thin Solid Films **517**, 6671 (2009).
[65] C. Walcott, *Animal Migration, Navigation, and Homing* (Springer-Verlag, New York, 1978), pp. 143–151.
[66] T. Alerstam, J. Exp. Biol. **130**, 63 (1987).
[67] A. Lednor and C. Walcott, Behav. Ecol. Sociobiol. **130**, 3 (1988).